Journal of Alloys and Compounds xxx (2008) xxx–xxx

Contents lists available at ScienceDirect

Journal of Alloys and Compounds

journal homepage: www.elsevier.com/locate/jallcom

Hydrothermal synthesis and characterization of self-assembled h-WO_3 nanowires/nanorods using EDTA salts

Jang-Hoon Ha, P. Muralidharan, Do Kyung Kim *

Department of Materials Science and Engineering, Korea Advanced Institute of Science and Technology (KAIST), 373-1 Guseong-dong, Yuseong-gu, Daejeon 305-701, Republic of Korea

ARTICLE INFO

Article history:
Received 9 May 2008
Received in revised form 9 July 2008
Accepted 10 July 2008
Available online xxx

Keywords:
Nanostructured materials
Oxide materials
Chemical synthesis
Electrochemical reactions
Transmission electron microscope

ABSTRACT

One-dimensional (1D) self-assembled single-crystalline hexagonal tungsten oxide (h-WO_3) nanostructures were synthesized by a hydrothermal method at 180 °C using sodium tungstate, ethylenediaminetetraacetic (EDTA) salts of sodium or ammonium, and sodium sulfate. Controlled morphological modification of h-WO_3 nanowire bundles was achieved and hierarchical urchin-like structures were produced by simply substituting the sodium ions with ammonium ions in the EDTA salt solution. Self-assembled h-WO_3 nanowire bundles and nanorods that formed urchin-like structures were characterized by X-ray diffraction (XRD), scanning electron microscopy (SEM), and transmission electron microscopy (TEM) techniques. 1D self-assembled h-WO_3 nanowire bundles of ~100 nm diameter and 1–2 μm length were comprised of several individual uniform nanowires of 4–6 nm diameter. These individual nanowires served as building blocks of the bundles. Raman, cyclic voltammetry (CV), and photoluminescence (PL) spectroscopy studies revealed their structure, electrochemical response, and luminescence properties. The synthesis of 1D self-assembled h-WO_3 nanowire bundles and urchin-like structures was differentiated by means of Na^+- and NH_4^+-based EDTA salt solutions.

1. Introduction

One-dimensional (1D) transition metal oxide nanostructures (nanowires, nanotubes, nanoribbons, and nanofibers) prepared via self-assembly have attracted considerable interest due to their high aspect-ratio structure, large surface areas, and unique physical properties, including optical, magnetic, and electronic characteristics [1,2]. Among the various transition oxides, tungsten oxide has received wide attention owing to its distinctive photo- and electrochromic properties [3–6]. It is considered a promising material for a multitude of potential applications including semiconductor gas sensors, electrode materials for secondary batteries, solar-energy devices, photocatalysts, erasable optical storage devices, and field-emission devices [6–11]. In particular, the hexagonal form of tungsten trioxide (h-WO_3), is of great interest due to its unique tunnel structure, and it has been widely used as an intercalation host to produce tungsten oxide bronzes, by the insertion of electrons and protons or metal ions like Li^+, Na^+, K^+, Zn^{2+}, etc. into the WO_3 structure.

Synthesis of single-crystalline 1D tungsten oxide nanostructures by heat treatment of tungsten foil, covered by a SiO_2 plate, in an argon atmosphere at 1600 °C has been reported [12]. In another approach, a tungsten tip was electrically etched and then heat treated at 700 °C under argon to yield a 1D nanostructure [13]. Recently, many researchers have attempted to develop methods to grow pure 1D tungsten oxide nanostructures at low temperature through solution-based and shape-controlled self-assembly routes.

In the literature [7,14–18], the synthesis of tungsten oxide nanostructure rods, wires, and belts has been reported by various reaction methods, including electrochemical techniques, template directed synthesis, chemical vapor deposition, solvo- and hydrothermal reaction, solution-based colloidal approach, and sonochemistry processes. Among them, solvo- and hydrothermal processes offer significant advantages, such as total control over their shape and size, low processing temperature, high homogeneity, cost effectiveness, and easy synthesis. High quality samples can be obtained by utilizing solvents under high pressures and temperatures to increase the solubility of the solid and to enhance the rate of the reaction. Kim and co-workers [14] utilized the solvothermal process with an alcohol and water mixture to synthesize highly oriented WO_3 nanowires and bundles. In addition, Gu et al. [15] reported the synthesis of WO_3 nanowire bundles, urchin-like, and ribbon-like superstructures based on 1D nanoscale building blocks by adding different sulfates with oxalic acid under hydrothermal conditions. According to their reports, the specific interaction between the sulfates and the crystal surfaces in presence of oxalic

* Corresponding author. Tel.: +82 42 8694118; fax: +82 42 8693310.
E-mail address: dkkim@kaist.ac.kr (D.K. Kim).

0925-8388/$ – see front matter © 2008 Elsevier B.V. All rights reserved.
doi:10.1016/j.jallcom.2008.07.048

acid has played a vital role to produce hierarchical structures of 1D WO_3 nanocrystals. Recently, ethylenediaminetetraacetic (EDTA) has been effectively employed in the hydrothermal process as a chelating ligand and capping reagent to produce 1D nanostructures of α-Bi_2O_3, YVO_4, $CeVO_4$, and $LaVO_4$:Eu^{3+} rods [19–22]. As a result, the importance of EDTA as a structure-directing agent under hydrothermal conditions has focused our interest to utilize EDTA in the synthesis of 1D h-WO_3 nanocrystals with different morphologies. Therefore, the present work investigates the synthesis of 1D self-assembled h-WO_3 nanocrystals using sodium and ammonium ions based EDTA salt solutions. Also, it is intended to identify the experimental parameters that control the morphology of WO_3 nanowire and/or urchin-like structures.

In this paper, the authors report on the synthesis of 1D h-WO_3 nanostructure using EDTA salt solutions and sodium sulfate through a simple hydrothermal process. The process facilitates control over the shapes of nanowire bundles and nanorods, allowing the formation of urchin-like crystalline h-WO_3 via simple substitution of NH_4^+ in place of Na^+ ions of EDTA salt solutions.

2. Experimental procedure

The analytical grade precursor chemicals used were sodium tungstate dihydrate ($Na_2WO_4{\cdot}2H_2O$, 99% Aldrich), ethylenediaminetetraacetic acid ($(HOOCCH_2)_2NCH_2{-}CH_2N(CH_2COOH)_2$, Junsei), sodium hydroxide (NaOH, Shinyo), ammonium hydroxide solution (NH_4OH, 25%, Fluka), sodium sulfate (Na_2SO_4), hydrochloric acid (HCl), and deionized (DI) water. All chemicals were used without further purification.

In a typical procedure to prepare the h-WO_3 nanorods, 1.84 g (0.0055 mol) $Na_2WO_4{\cdot}2H_2O$ was dissolved in 10 mL of DI water under stirring. The clear solution was slowly acidified to a pH range of 1–1.2 using 10 mL of 3 M HCl under continuous stirring to form a pale yellow precipitate. EDTA salt solution was prepared by dissolving EDTA and sodium hydroxide in 50 mL of DI water under continuous stirring. Subsequently, the clear EDTA sodium salt solution was added to the tungsten acid precipitated solution and diluted to 80 mL, and a specified amount of sodium sulfate (1.25–5 g) was added. 80 mL of the mixed slurry solution was transferred to a 100-mL Teflon-lined stainless steel autoclave and hydrothermal reaction proceeded at 140–180 °C for 4–12 h in a preheated electric oven. After the reaction, the final products were washed sequentially with DI water and ethanol to remove the sulfate ions and other remnants by centrifugation. The obtained powder was subsequently dried at 60 °C for 12 h in air. In the above procedure, NH_4OH was added instead of NaOH to form an ammonium-based EDTA salt solution and an excess amount (i.e. 20 mL) of 3 M HCl was added to maintain the pH in a range of 1–1.2. The other conditions were held unchanged to prepare self-assembled nanorods that form urchin-like h-WO_3 nanostructures.

The synthesized h-WO_3 nanostructures were characterized using an X-ray diffractometer (XRD, Rigaku, D/max-IIIC X-ray diffractometer, Tokyo, Japan) with Cu Kα radiation (λ = 0.15406 nm at 40 kV and 45 mA). The sizes and shapes of the nanostructures were observed on a field emission scanning electron microscope (FE-SEM Philips XL30 FEG, Eindhoven, Netherland), a high-resolution transmission electron microscope (HR-TEM, JEM 3010, JEOL, Tokyo, Japan), and micro-Raman spectroscopy (LABRAM, Jobin-Yvon, France) using a 514.5 nm—line Ar ion laser in a backscattering geometry, where the laser power at the sample location was set at 1 mW. Cyclic voltammetry (CV) was performed in a classical three electrode electrochemical cell within ±0.8 V for WO_3 film deposited on an ITO-coated glass substrate, by dipping the ITO-coated glass into a highly dispersed nanostructured h-WO_3 in DI water. A single-compartment cell was configured with three electrodes: an h-WO_3 layer on an ITO-coated glass substrate acted as a working electrode, a platinum wire was used as an auxiliary electrode, and an Ag/AgCl was used as a reference electrode and the electrolyte was 0.1 M H_2SO_4. The fabricated electrochemical cell was connected to a potentiostat/galvanostat (Princeton Applied Research 263A, TN, USA) controlled by a computer program. The photoluminescence (PL) spectra were recorded for the h-WO_3 nanostructures using a photoluminescence spectrometer (PS-PLUI-XWP1400, Seoul, Korea) equipped with a 500-W Xe arc-lamp under excitation at 275 nm.

3. Results and discussion

Nanowire bundles and urchin-like structure crystalline h-WO_3 samples were synthesized through hydrothermal reaction of $Na_2WO_4{\cdot}2H_2O$, HCl and Na^+- or NH_4^+-based EDTA salt solutions in the presence of Na_2SO_4. The XRD patterns for the as-synthesized h-WO_3 powders using Na^+ ion- and NH_4^+ ion-based EDTA salt solutions are shown in Fig. 1. For the as-synthesized h-WO_3 with Na^+-based EDTA, intense and sharp diffraction peaks (Fig. 1a) are observed, indicative of high-degree crystallinity. On the other hand, the as-synthesized h-WO_3 with the NH_4^+-based EDTA sample showed broader peaks with less intensity (Fig. 1b). It is also observed that there are no other impurity phase peaks. The diffraction peaks can be indexed to the pure hexagonal phase of WO_3 with lattice constants of a = 7.2614 Å and c = 3.859 Å, which agrees well with the reported values of a = 7.298 Å, c = 3.899 Å, space group $P6/mm$ from the JCPDS card # 33-1387, as shown in Fig. 1.

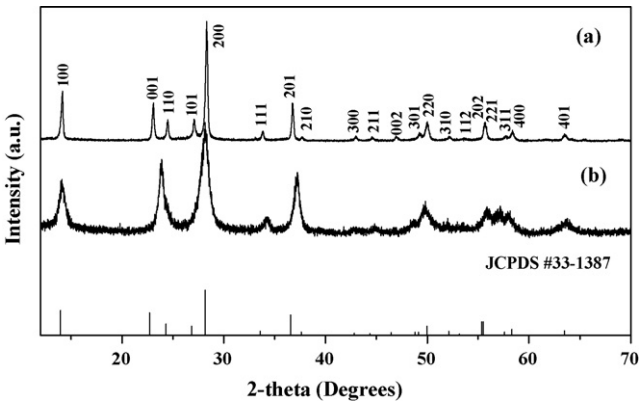

Fig. 1. XRD patterns of h-WO_3 nanopowders: (a) nanowire bundles (Na^+-based EDTA), (b) urchin-like (NH_4^+-based EDTA) and (c) JCPDS card # 33-1387, hydrothermally synthesized at 180 °C for 8 h.

SEM micrographs presented in Fig. 2 show the as-synthesized h-WO_3 utilizing Na^+ ion- and NH_4^+ ion-based EDTA salt solutions via the hydrothermal method at 180 °C for 4 h and 8 h, respectively. It is observed in Fig. 2b that the self-assembled nanowires formed nanowire bundles as a result of the synthesis approach using Na^+-based EDTA salt solution. Alternatively, numerous nanorods were self-assembled to form an urchin-like microspherical (Fig. 2e) structure by the addition of NH_4^+-based EDTA in place of Na^+-based EDTA, while the other conditions were maintained the same. Highly oriented 1D nanowires were self-assembled to form nanowire bundles of h-WO_3 having a diameter of 100–150 nm and length of 1.5–2.5 μm, with individual nanowires of ~4–6 nm diameter (Fig. 2b). It is observed in Fig. 2b that the single-crystalline 1D h-WO_3 nanowire bundles with a flat tip end had formed after reaction for 8 h. The low magnification SEM image in Fig. 2c shows the large area distribution of uniform nanowire bundles. Urchin-like microsphere structures (Fig. 2e) ~2 μm in diameter were formed by self-assembly of numerous nanorods. The surfaces of these microsphere structures were covered by numerous nanorods such that they take on the appearance of urchin-like structures, and the composed individual nanorods measured ~5–20 nm in diameter. The energy dispersive X-ray (EDX) spectrum presented in Fig. 2f reveals a 3:1 molar ratio for oxygen and tungsten elements, which solely constitute the composition of the h-WO_3 nanorods/nanowires.

In order to elucidate the h-WO_3 self-assembled nanostructure growth process, hydrothermal experiments were carried out under various reaction conditions. The SEM image (Fig. 2a) showed that a mixture of aggregated short nanowire bundles and short nanorods was formed after 4 h of reaction time at 180 °C. On the other hand, the reaction conducted at 180 °C for 8 h revealed the formation of uniform self-assembled nanowire bundles (Fig. 2b and c). The SEM image in Fig. 2d of h-WO_3 synthesized using the NH_4^+-based EDTA solution at 180 °C for 4 h reveals smaller spheres of 100~200 nm size with irregular short nanorods grown from the surface of the spheres compared to the product formed after 8 h reaction time. Hence, it can be concluded from the above results that the for-

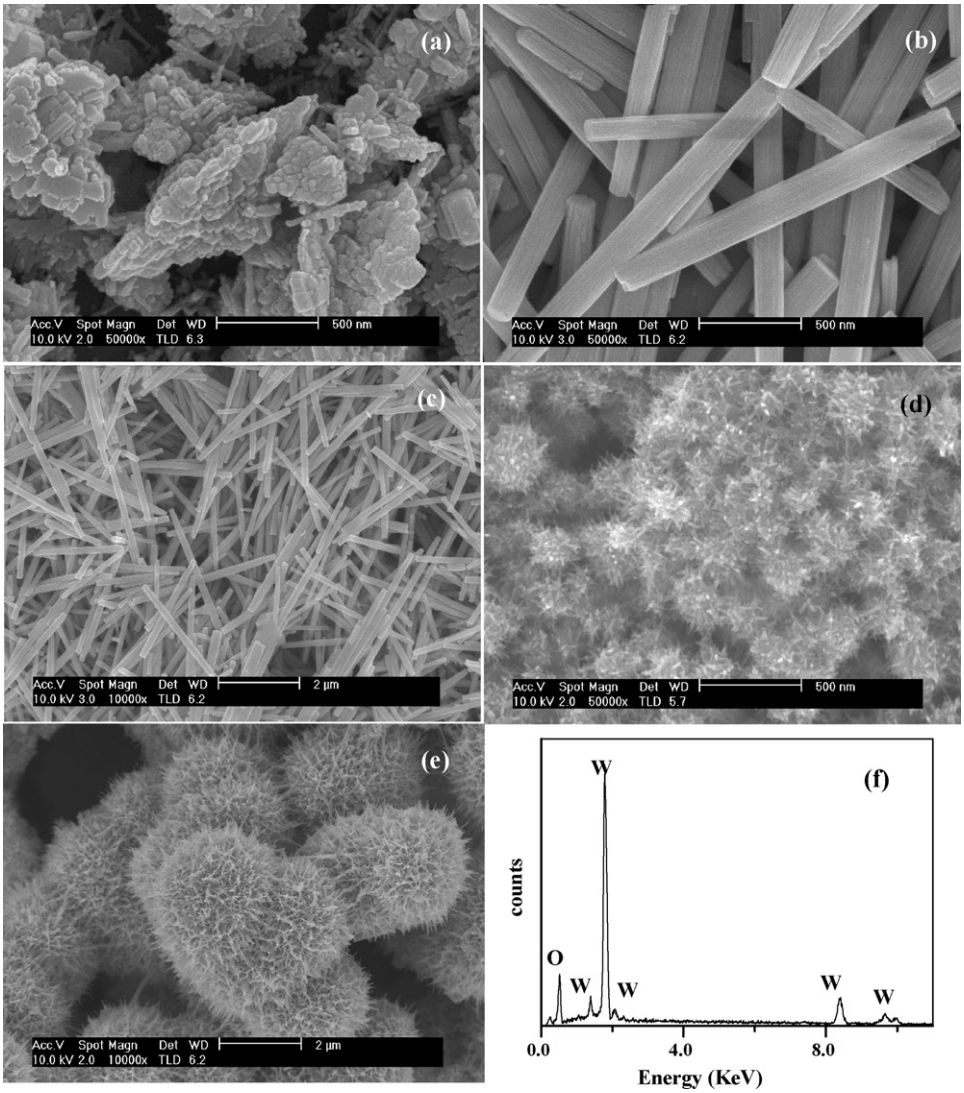

Fig. 2. SEM images of h-WO_3 nanowires bundles synthesized at 180 °C: (a) 4 h, (b) 8 h (higher magnification) and (c) 8 h (lower magnification), and urchin-like structure synthesized at 180 °C (d) 4 h, and (e) 8 h, and (f) the EDX spectrum of h-WO_3.

mation of highly self-assembled nanostructures, such as nanowire bundles and urchin-like structures, requires a minimum reaction time to form a stable coordination complex with EDTA in aqueous solution. It is clear that a strong ligand (EDTA) is not only needed to form a stable complex with W^{6+}, but also the ligand binds to the surface of the crystal, which directly affects the growth direction and crystal structure of the nanocrystals. The growth process is considered to be similar to that reported by Gu et al. [15]. Specifically, there appear to be two intermediates associated with two growth stages: the growth of aggregate particles is facilitated and followed by the growth of 1D nanorods to form the urchin-like structure.

TEM and HR-TEM micrographs of h-WO_3 nanostructures formed using Na^+ ion- and NH_4^+ ion-based EDTA salt solutions are shown in Fig. 3. It is observed that self-assembled nanowires form uniform rod-shaped nanowire bundles. The bundle is comprise of several nanowires with uniform diameter of about 4–6 nm along their entire length. The image shows clear individual nanowires in the nanowire bundles. It is observed that self-assembled nanorods formed an urchin-like structure, as shown in Fig. 3c. Nanorods with uniform diameter of about 8–10 nm are observed. Furthermore, the image shows the clear individual nanorods dispersed from the urchin-like structure. HR-TEM images of the h-WO_3 nanowire bundles and nanorods in urchin-like formations are shown in Fig. 3b and d. Here, the spacing of the lattice fringes is 0.384 nm and 0.375 nm, respectively. The plane of the spacing of lattice fringes was indexed as (0 0 1) for the h-WO_3 nanostructure, which confirms that the nanostructures are grown along the *c*-axis direction, which is in agreement with JCPDS card #33-1387.

From sequential experimental studies, it is evident that Na^+ ion- and NH_4^+ ion-based EDTA solutions play an important role in the construction of h-WO_3 nanostructures with controlled morphology. The experimental results obtained under varying parameters showed that Na_2SO_4 also plays a vital role in the formation of self-assembled nanostructures. In the present work, both nanowire bundles and nanorods formed urchin-like structures in the presence of Na_2SO_4 with EDTA. In contrast, controlled structural morphologies of nanowire bundles and nanorods characterized by urchin-like structures were only obtained by substituting the Na^+ and NH_4^+ ions of the EDTA salt solutions. In the absence of EDTA or Na_2SO_4, only irregular nanoparticles were obtained. As reported in the literature [19–22], EDTA has been widely used as for chelating, capping, and as a structure-directing template in the synthesis of 1D nanostructured materials. Thus, it appears that Na^+-or NH_4^+-based

Please cite this article in press as: J.-H. Ha, et al., J. Alloys Compd. (2008), doi:10.1016/j.jallcom.2008.07.048

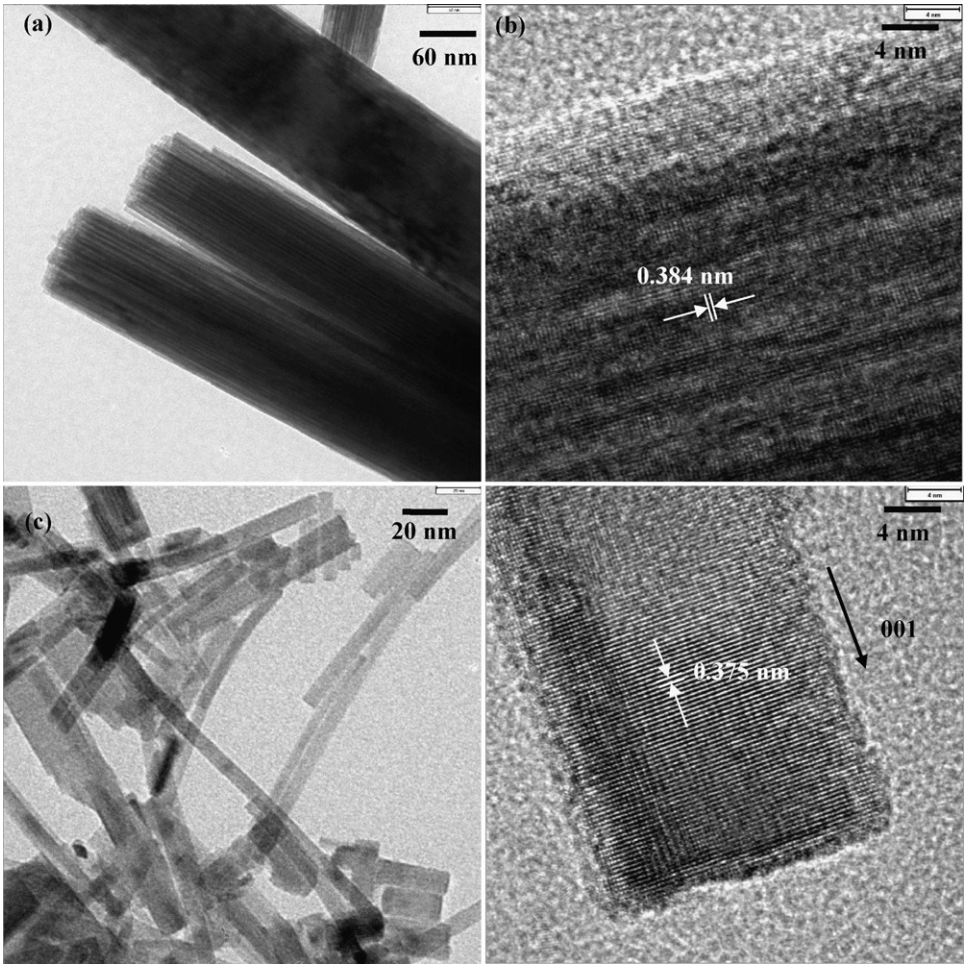

Fig. 3. TEM images of h-WO_3: (a) nanowire bundles (b) HR-TEM images of individual nanowire bundles, (c) TEM images of nanorods forming urchin-like structure and (d) HR-TEM images of individual nanorods, hydrothermally synthesized at 180 °C for 8 h.

EDTA salt can induce and significantly enhance the structure-directing role of sulfates in the preparation of self-assembled tungsten oxide nanostructures. In another approach, experiments have revealed that reactions carried out with ammonium tungstate and a NH_4^+ ion-based EDTA salt solution and $(NH_4)_2SO_4$ yielded irregular particles. In addition, reactions were carried using sodium tungstate, Na^+-based EDTA, and $(NH_4)_2SO_4$ precursors, also resulting in the formation of irregular particles. The total absence of sodium ions in the reaction medium or sodium sulfate leads to the formation of irregular particles. Therefore, the overall experimental parameters require a particular amount of sodium ions in the reaction medium for producing the needed morphology of h-WO_3 nanocrystals. Thus, the sodium ions in the reaction medium play a unique role even though presence of ammonium ions is required for producing the morphology of urchin-like structure of WO_3 nanocrystals. The present work, therefore, uses sodium tungstate, Na^+ ion-, and NH_4^+ ion-based EDTA salts in the presence of Na_2SO_4 to yield self-assembled nanowire bundles and nanorods in the formation of urchin-like structures, respectively. From the above results, EDTA salt solutions of Na^+ and NH_4^+ ions were found to play an important role in controlling the different morphologies and microstructures.

Raman spectra for the as-synthesized nanowire bundles and urchin-like structures of the h-WO_3 are shown in Fig. 4. Well-defined Raman peaks centered at 242 cm^{-1}, 325 cm^{-1}, 668 cm^{-1}, 754 cm^{-1}, and 810 cm^{-1} can be observed. According to the literature [23,24], these bands can be assigned to the fundamental modes of crystalline h-WO_3. The bands at 754 cm^{-1} and 810 cm^{-1} in Fig. 4a are related to O–W–O stretching modes, while the bands at 242 cm^{-1} and 325 cm^{-1} can be attributed to the W–O–W bend-

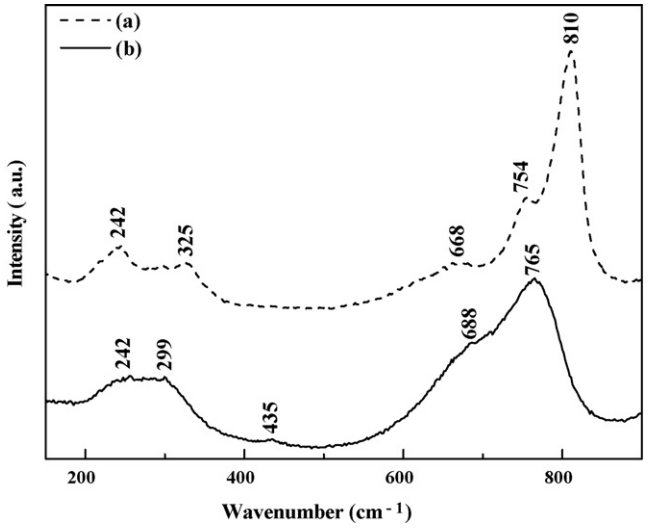

Fig. 4. Raman spectra of h-WO_3: (a) nanowire bundles and (b) urchin-like structures synthesized at 180 °C for 8 h.

Please cite this article in press as: J.-H. Ha, et al., J. Alloys Compd. (2008), doi:10.1016/j.jallcom.2008.07.048

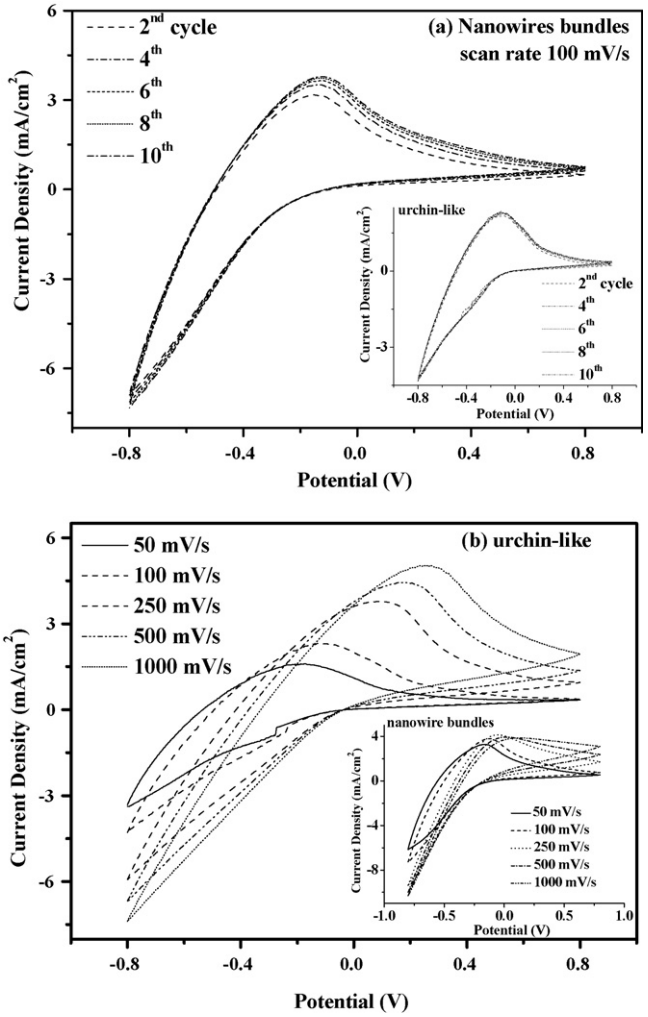

Fig. 5. Cyclic voltammograms of (a) h-WO_3 nanowire bundles, and inset Figure, CV curves of urchin-like, were measured in 0.1 M H_2SO_4 at a scan rate of 100 mV/s for 10 cycles and (b) CV curves of h-WO_3 urchin-like structures, and inset Figure, CV curves of nanowire bundles, were measured at various scan rates of 50 mV/s, 100 mV/s, 250 mV/s, 500 mV/s, and 1000 mV/s during the 10th cycles.

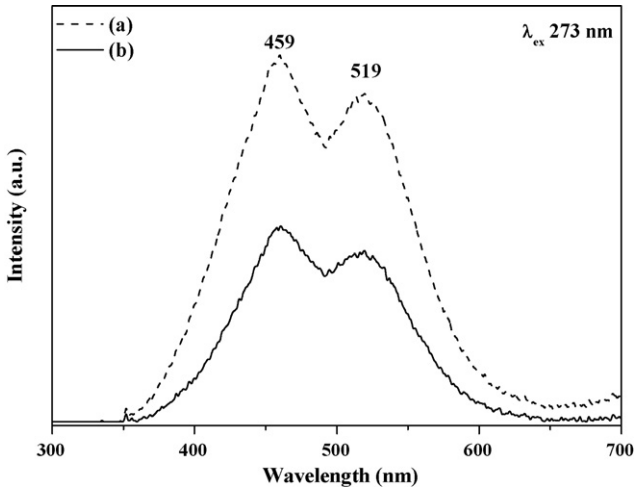

Fig. 6. Photoluminescence spectra of h-WO_3 powders: (a) nanowire bundles and (b) urchin-like structures hydrothermally synthesized at 180 °C for 8 h.

ing mode of the bridging oxygen. The band at 435 cm^{-1} can be attributed to the characteristic band of crystalline WO_3 [23]. Broadened and slightly shifted Raman peaks at 224 cm^{-1}, 302 cm^{-1}, 680 cm^{-1} and 765 cm^{-1} are observed for the urchin-like structure sample presented in Fig. 4b. The fundamental cause of the shift might be related to the hierarchical urchin-like nanostructure with the existence of oxygen deficiency [25]. Further investigations of this aspect should be undertaken. In both the nanowires and nanorods, a weak shoulder at ~660 cm^{-1} is observed. This could be assigned to O–W–O stretching vibration of the bridging oxygen in the residual hydrated tungsten oxide due to the absence of a high-temperature post-heat treatment step [26].

Cyclic voltammograms of nanowire bundles and urchin-like structures of h-WO_3 layer on an ITO-coated glass substrates were measured at various scan rates of 50 mV/s, 100 mV/s, 250 mV/s, 500 mV/s, and 1000 mV/s for a continuous number of cycles. The voltammogram curves were sweeped in potential ranges from −0.8 V to +0.8 V for the h-WO_3 layer on ITO-coated glass having a working electrode. The voltammogram curves in Fig. 5 show the electrochemical response of the nanowire bundles measured at a scan rate of 100 mV/s for the first 10 cycles. The CV curves in Fig. 5b, and inset were measured during the 10th cycle at various scan rates for the urchin-like sample comprised of nanorods and nanowire bundles, respectively. The obtained results are similar to those reported [27–29] in previous studies of proton insertion in tungsten oxide. h-WO_3 exhibited a good electrochemical response without any delamination of film into the acidic solution. There is an anodic current peak at −0.13 V for the nanowire bundles (Fig. 5a) and at 0.11 V for the urchin structure (inset Fig. 5a) sample. The current response was stable without significant change in shape, indicating excellent cycling stability of the nanowires bundles and urchin structure, even in acidic solution. It is observed in Fig. 5 that cathodic current increased rapidly at about −0.8 V and an anodic current peak appeared in the potential range of about −0.4 to +0.05 V, centered at −0.13 V. The rapid increase in cathodic current is associated with the evolution of hydrogen on the WO_3 film and the anodic current peak is due to the oxidation of hydrogen insertion into the WO_3 film. It is to note that anodic current peak was slightly shifted to anodic potential as the number of cycle increased. It is possible that the insertion of hydrogen is located initially at reversibly active site for a moment and then is located at reversible trap site in order to bind inserted hydrogen relatively stronger than reversibly active site. Upon continuous number of cycles, the amount of hydrogen located at reversible trap site increases and the role of reversible trap site in the hydrogen insertion into the WO_3 film is more significant as a result, anodic current peak slightly shifts in the anodic direction. The CV curves shown in Fig. 5b reveal anodic current peak with the peak potential shifted to more positive potentials from −0.19 V to 0.26 V for measurement preformed at different scan rates of 50 mV/s, 100 mV/s, 250 mV/s, 500 mV/s, and 1000 mV/s. On the other hand, in the case of the nanowire bundles, there is a slight shift in the CV curves from −0.15 V to 0.09 V with an increase in the scan rate (inset Fig. 5b). From the above results, it can be concluded that the urchin-like structure experiences slow insertion kinetics, leading to irreversibility. Thus, the CV results of the nanowire bundles revealed a good electrochemical reversibility of the electrode for continuous number of cycles at various scan rates.

The PL spectra for the nanowire bundles and urchin-like structure of h-WO_3 synthesized using Na^+ ion- and NH_4^+ ion-based EDTA salt solution are shown in Fig. 6. The two strongest PL emission peaks are centered at 2.69 eV (459 nm) and 2.39 eV (518 nm) for the nanowire bundles and at 2.69 eV (460 nm) and 2.38 eV (518 nm) for the urchin-like structure. The PL emission spectra show a characteristic blue emission peak at 2.69 eV (459 nm), and increased

Please cite this article in press as: J.-H. Ha, et al., J. Alloys Compd. (2008), doi:10.1016/j.jallcom.2008.07.048

intensity of this peak was observed for the nanowire bundles compared to the nanorods forming an urchin-like structure. It has been well known that the size and shape of nanomaterials affect the physicochemical properties. In the literature [30], similar PL spectra with two emission maxima at lower energies of 2.8 eV and 2.3 eV were reported for a thin film of a WO_3 system at 80 K. However, the emission peak at higher energy (2.8 eV) disappeared at room temperature. This was attributed to electron-hole radiative recombination, and the lower-energy peak was assigned to localized states in the band gap due to impurities. The blue emission characterized by the PL spectra at room temperature for nanowire bundles and urchin-like structure of WO_3 are well agreed with the literature reports [31–34]. In this study, it could be suggested that the emissions of the nanowire bundles and nanorods samples may possibly correspond to trap-state emission. During the process, each oxygen vacancy would trap one electron from the transition level of a tungsten atom to become an ionized oxygen vacancy. As the process involved reduction reaction, many ionized oxygen vacancies are expected to form. At the same time, W atoms, which contribute electrons to the trap state, tend to form the most stable WO_3 phase to charge balance the cation–anion relationship. The blue emission of nanorods might have originated from the presence of oxygen vacancies or defects in the nanowire bundles resulting from faster 1D crystal growth, and hence the high intense PL emission would be associated with the presence of defects.

4. Conclusions

Self-assembled 1D h-WO_3 nanowire bundles and urchin-like structures were successfully synthesized through a hydrothermal process. A pure hexagonal phase crystalline WO_3 hierarchical nanostructure was confirmed by XRD and TEM analyses. SEM and TEM images revealed self-assembled nanowire bundles and nanorods that formed urchin-like structures. The shapes of the h-WO_3 nanowire bundles and urchin-like nanostructures could be manipulated by application of Na^+- and NH_4^+-based EDTA salt solutions in the presence of Na_2SO_4. In addition, a particular amount of sodium ions in the reaction medium plays a unique role even though presence of ammonium ions is required for producing the morphology of urchin-like structure of WO_3 nanocrystals. This versatile method provides a straightforward and efficient means of obtaining WO_3 nanostructures having unique morphologies. The characteristic properties of the nanowire bundles were considerably enhanced compared to those of the urchin-like structures, because of their highly ordered self-assembled structures.

Acknowledgement

This work was supported by a Korea Research Foundation Grant funded by the Korean Government (MOEHRD) (KRF-2005-005-J09701).

References

[1] C.N.R. Rao, F.L. Deepak, G. Gundiah, A. Govindaraj, Prog. Solid State Chem. 31 (2003) 5–147.
[2] G.R. Patzke, F. Krumeich, R. Nesper, Angew. Chem. Int. Ed. 41 (2002) 2446–2461.
[3] S.J. Yoo, J.W. Lim, Y.E. Sung, Y.H. Jung, H.G. Choi, D.K. Kim, Appl. Phys. Lett. 90 (2007) 173126–173133.
[4] T. He, Y. Ma, Y.A. Cao, W.S. Yang, J.N. Yao, Phys. Chem. Chem. Phys. 4 (2002) 1637–1639.
[5] Y.M. Lu, C.P. Hu, J. Alloy. Compd. 449 (2008) 389–392.
[6] S. Nagata, A. Inouye, S. Yamamoto, B. Tsuchiya, K. Takano, K. Toh, T. Shikama, J. Alloy. Compd. 446 (2007) 558–561.
[7] X.L. Li, J.F. Liu, Y.D. Li, Inorg. Chem. 42 (2003) 921–924.
[8] L.G. Teoh, J. Shieh, W.H. Lai, I.M. Hung, M.H. Hon, J. Alloy. Compd. 396 (2005) 251–254.
[9] T. He, Y. Ma, Y. Cao, X.L. Hu, H.M. Liu, G.J. Zhang, W.S. Yang, J. Yao, J. Phys. Chem. B 106 (2002) 12670–12676.
[10] M. Hibino, W.C. Han, T. Kudo, Solid State Ionics 135 (2000) 61–69.
[11] B. Zhang, J.D. Liu, S.K. Guan, Y.Z. Wan, Y.Z. Zhang, R.F. Chen, J. Alloy. Compd. 439 (2007) 55–58.
[12] Y.Q. Zhu, W.B. Hu, W.K. Hsu, M. Terrones, N. Grobert, J.P. Hare, H.W. Kroto, D.R.M. Walton, H. Terrones, Chem. Phys. Lett. 309 (1999) 327–334.
[13] G. Gu, B. Zheng, W.Q. Han, S. Roth, J. Liu, Nano Lett. 2 (2002) 849–851.
[14] H.G. Choi, Y.H. Jung, D.K. Kim, J. Am. Ceram. Soc. 88 (2005) 1684–1686.
[15] Z.J. Gu, T.Y. Zhai, B.F. Gao, X.H. Sheng, Y.B. Wang, H.B. Fu, Y. Ma, J. Yao, J. Phys. Chem. B 110 (2006) 23829–23836.
[16] X.W. Lou, H.C. Zeng, Inorg. Chem. 42 (2003) 6169–6171.
[17] N. Shankar, M.F. Yu, S.P. Vanka, N.G. Glumac, Mater. Lett. 60 (2006) 771–774.
[18] J.G. Yuan, Y.Z. Zhang, J. Le, L.X. Song, X.F. Hu, Mater. Lett. 61 (2007) 1114–1117.
[19] Y. Xiong, M.Z. Wu, J. Ye, Q.W. Chen, Mater. Lett. 62 (2008) 1165–1168.
[20] J. Ma, Q.S. Wu, Y.P. Ding, Mater. Lett. 61 (2007) 3616–3619.
[21] F. Luo, C.J. Jia, W. Song, L.P. You, C.H. Yan, Cryst. Growth Des. 5 (2005) 137–142.
[22] N. Wang, W. Chen, Q.F. Zhang, Y. Dai, Mater. Lett. 62 (2008) 109–112.
[23] M.F. Daniel, B. Desbat, J.C. Lassegues, B. Gerand, M. Figlarz, J. Solid State Chem. 67 (1987) 235–247.
[24] G.L. Frey, A. Rothschild, J. Sloan, R. Rosentsveig, R. Popovitz-Biro, R. Tenne, J. Solid State Chem. 162 (2001) 300–314.
[25] D. Bersani, G. Antonioli, P.P. Lottici, T. Lopez, J. Non-Cryst. Solids 234 (1998) 175–181.
[26] C. Santato, M. Odziemkowski, M. Ulmann, J. Augustynski, J. Am. Chem. Soc. 123 (2001) 10639–10649.
[27] A.C. Dillon, A.H. Mahan, R. Deshpande, R. Parilla, K.M. Jones, S.H. Lee, Thin Solid Films 516 (2008) 794–797.
[28] C. Balazsi, L. Wang, E.O. Zayim, I.M. Szilagyi, K. Sedlackova, J. Pfeifer, A.L. Toth, P.I. Gouma, J. Eur. Ceram. Soc. 28 (2008) 913–917.
[29] D.-J. Kim, S.I Pyun, Solid State Ionics 99 (1997) 185–192.
[30] M. Manfredi, G.C. Paracchini, G. Schianchi, Thin Solid Films 79 (1981) 161–166.
[31] C. Paracchini, G. Schianchi, Phys. Status Solidi A 72 (1982) K129–K132.
[32] K. Lee, W.S. Seo, J.T. Park, J. Am. Chem. Soc. 125 (2003) 3408–3409.
[33] K. Woo, J. Hong, J.-P. Ahn, J.-K. Park, K.-J. Kim, Inorg. Chem. 44 (2005) 7171–7174.
[34] M.-T. Chang, L.-J. Chou, Y.-L. Chueh, Y.-C. Lee, C.-H. Hsieh, C.-D. Chen, Y.-W. Lan, L.-J. Chen, Small 3 (2007) 658–664.